

AFIT/GNE/ENP/92D-1

AD-A270 456



DTIC
ELECTE
OCT 12 1993
S A D

TOTAL HEMISPHERICAL EMITTANCE
OF NIOBIUM-1% ZIRCONIUM FUEL CLADDING
FOR THE SP-100 SPACE REACTOR
THESIS

John E. Thomason, III

AFIT/GNE/ENP/92D-1

Approved for public release; distribution unlimited

93 10 7 0 8 8

93-23830



71p8

REPORT DOCUMENTATION PAGE			Form Approved OMB No 0704-0188	
<small>Public reporting burden for this collection of information is estimated to average 1 hour per response, including the time for reviewing instructions, searching existing data sources, gathering and maintaining the data needed, and completing and reviewing the collection of information. Send comments regarding this burden estimate or any other aspect of this collection of information, including suggestions for reducing this burden, to Washington Headquarters Services, Directorate for Information Operations and Reports, 1215 Jefferson Davis Highway, Suite 1204, Arlington, VA 22202-4302 and to the Office of Management and Budget, Paperwork Reduction Project (0704-0188), Washington, DC 20503</small>				
1. AGENCY USE ONLY (Leave blank)		2. REPORT DATE December 1992		3. REPORT TYPE AND DATES COVERED Master's Thesis
4. TITLE AND SUBTITLE TOTAL HEMISPHERICAL EMITTANCE OF NIOBIUM - 1% ZIRCONIUM FUEL CLADDING FOR THE SP-100 SPACE REACTOR			5. FUNDING NUMBERS	
6. AUTHOR(S) JOHN E. THOMASON, III				
7. PERFORMING ORGANIZATION NAME(S) AND ADDRESS(ES) AIR FORCE INSTITUTE OF TECHNOLOGY WRIGHT-PATTERSON AFB, OH 45433			8. PERFORMING ORGANIZATION REPORT NUMBER AFIT/GNE/ENP/92D-1	
9. SPONSORING / MONITORING AGENCY NAME(S) AND ADDRESS(ES)			10. SPONSORING / MONITORING AGENCY REPORT NUMBER	
11. SUPPLEMENTARY NOTES				
12a. DISTRIBUTION / AVAILABILITY STATEMENT Approved for public release; distribution unlimited.			12b. DISTRIBUTION CODE	
13. ABSTRACT (Maximum 200 words) Total hemispherical emittance was measured for the SP-100 reactor fuel cladding alloy (Nb-1% Zr). Based on a standard test method (ASTM C 835-82), experiments were conducted on a reference sample of oxidized stainless steel and then on a sample of actual cladding. The sample is heated in a vacuum by passing DC current through it until reaching equilibrium. Measurements are made of the electrical power dissipated in the sample and of the surface temperature. Using the Stefan-Boltzmann Law and some key assumptions concerning conductive and radiative heat transfer, the measured quantities are used to calculate emittance. Calculated values for unoxidized cladding range from $0.159 \pm 1.34\%$ at 913 K to $0.200 \pm 1.25\%$ at 1091 K. Highest value measured after onset of visible oxidation was $0.339 \pm 1.63\%$ at 1269 K.				
14. SUBJECT TERMS SP-100, reactor, emittance, niobium, fuel cladding, emissivity			15. NUMBER OF PAGES 67	
			16. PRICE CODE	
17. SECURITY CLASSIFICATION OF REPORT Unclassified	18. SECURITY CLASSIFICATION OF THIS PAGE Unclassified	19. SECURITY CLASSIFICATION OF ABSTRACT Unclassified	20. LIMITATION OF ABSTRACT UL	

AFIT/GNE/ENP/92D-1

**TOTAL HEMISPHERICAL EMITTANCE
OF NIOBIUM-1½ ZIRCONIUM FUEL CLADDING
FOR THE SP-100 SPACE REACTOR**

THESIS

**Presented to the Faculty of the School of Engineering
of the Air Force Institute of Technology**

Air University

**In Partial Fulfillment of the
Requirements for the Degree of
Master of Science**

John E. Thomason, III, B.S.

Accession For		
NTIS	CRA&I	<input checked="checked" type="checkbox"/>
DTIC	TAB	<input type="checkbox"/>
Unannounced		<input type="checkbox"/>
Justification		
By		
Distribution /		
Availability Codes		
Dist	Avail and/or Special	
A-1		

December 1992

DTIC QUALITY INSPECTED 2

Approved for public release; distribution unlimited

Preface

The purpose of this study was to measure the total hemispherical emittance of the fuel cladding for the SP-100 space nuclear reactor core. The reason for measuring this property was to provide a more accurate emittance value for computer modeling of the consequences of a loss-of-coolant accident occurring in space. Although the emittance of Nb-1% Zr had been measured by others, there remained some degree of uncertainty concerning the possible effects of cladding geometry and core environment on the alloy's thermal radiation properties. This study was designed to provide a basis for conducting emittance research on the cladding by attempting to measure the emittance of an actual sample in a vacuum.

The method and apparatus for calculating emittance were based on a standard test method (ASTM C 835-82, Reapproved 1988). Although emittance was reported over the temperature range of about 900 to 1300 K, the more interesting region toward the upper core operating limit of 2000 K was not explored due to equipment limitations. In addition, the specimen was affected by gradual oxidation resulting from heating under a less-than-adequate vacuum, a condition which hampered statistical error analysis. Despite such limitations, the method provided conclusive results. With some procedural modifications and improved equipment, it appears promising for continued research.

I am extremely grateful to my advisor, Col Ronald Tuttle, for his engineering and logistics assistance. Thanks goes to Leroy Cannon and to Professors Robert Hengehold and George John for their assistance with ion and diffusion pump vacuum systems. The excellent fabrication support from Jack Tiffany and the AFIT Model Shop is appreciated. Special thanks goes to Dave McElroy and Tom Kollie of Oak Ridge National Laboratory for their technical guidance. Finally I would like to express my appreciation to my wife, Nancy, for her patience, support, and encouragement.

John E. Thomason, III

Table of Contents

	Page
Preface	ii
List of Figures	vi
List of Tables	vii
Notation	viii
Abstract	x
I. Introduction	1
Background	1
Definition of Emittance	3
Problem	4
Scope	6
Assumptions	7
Approach	8
II. Theory	9
Introduction	9
Stefan-Boltzmann Law	9
Heat Flow in a Solid Cylinder of Conducting Metal	10
Heat Flow in a Thin, Hollow Cylinder of Conducting Metal	13
III. Apparatus	18
The Basics	18
Vacuum System	18
Bell Jar	19
DC Power Supply	19
Precision Voltmeter	21
Specimen Holder	21
Thermocouples	21
IV. Experimental Procedure	28
Preparation	28
Data Collection	29
Data Reduction	31
V. Results	33
Introduction	33
SS Specimen Emittance Values	33

	Page
SS Specimen Error Analysis	35
Nb-1% Zr Specimen Emittance Values	36
Nb-1% Zr Specimen Error Analysis	37
VI. Summary and Recommendations	39
Summary	39
Recommendations	39
APPENDIX A: Temperature Correlations	44
APPENDIX B: Sample Data and Calculation Results	45
APPENDIX C: Estimation of Errors and Uncertainties	51
Bibliography	55
Vita	57

List of Figures

Figure	Page
1. Hemispherical Radiation from a Point on the Surface of a Cylinder	4
2. Overview of Apparatus	5
3. Axial Temperature Distribution Along an Electrically Heated Metallic Cylinder	14
4. Nb-1% Zr Specimen Mounted Inside Bell Jar	22
5. Thermocouple and Electrode Placement	23
6. Wiring Diagram for Thermocouple Number 1.	25
7. Wiring Diagram for Measuring Voltage Drop Across Specimen Between Thermocouples 1 and 2	26
8. Wiring Diagram for Measuring Voltage Drop Across Precision Resistor	27
9. Initial Results Compared to ORNL, Emittance vs Temperature, SS Specimen	33
10. SS Specimen Emittance Corrected for Thermocouple Calibration Error	35
11. Emittance vs Temperature--Nb-1% Zr	36

List of Tables

Table	Page
I. Power Series Expansion for emf of Type S Thermocouples	44
II. Power Series Expansion for ϵ of Nb-1% Zr	44
III. Sample Data--Stainless Steel	46
IV. Sample Data--Nb-1% Zr	47
V. Sample Initial Calculation Results-- Stainless Steel (Uncorrected)	48
VI. Sample Calculation Results--Stainless Steel (Corrected)	49
VII. Sample Calculation Results--Nb-1% Zr	50
VIII. Sample Uncertainty Estimation	54

Notation

<u>Symbol</u>	<u>Description</u>	<u>Units</u>
A	Area	m ²
c	Specific heat	J kg ⁻¹ K ⁻¹
D	Density	kg m ⁻³
E	Electric potential	volts [V]
e	Percent error	%
I	Current	amperes [A]
J	Bessel Function	
k	Separation constant	
n	Separation constant	
P	Power	watts [W]
R	Temperature (radial)	K
T	Absolute Temperature	K
Z	Temperature (axial)	K
z	Axial coordinate	
α	Absorptance	
δ	Maximum estimated error	
ϵ	Emittance	
Θ	Temperature (azimuthal)	K
θ	Angular coordinate	
ρ	Radial coordinate	
σ	Stefan-Boltzmann Constant (5.67051 X 10 ⁻⁸)	W m ⁻² K ⁻⁴

Subscripts

A	Absorbed
a	Per unit area
Cd	Conducted
Cv	Convected
D	Dissipated
H	Total Hemispherical
L	Per unit length
R	Radiated
S	Stored

Abstract

The purpose of this study was to measure the total hemispherical emittance of Nb-1% Zr fuel cladding for the SP-100 space nuclear reactor in the operational temperature range. An apparatus was constructed based primarily on ASTM C 835-82, Standard Test Method for Total Hemispherical Emittance of Surfaces from 20 to 1400° C (Reapproved 1988). The test method required heating the specimen in a vacuum until achieving thermodynamic equilibrium between the specimen and its surroundings. This was accomplished by passing an electric current through the specimen and then allowing its surface temperature to stabilize. Measurements were made of the surface temperature and the electric power dissipated within a predetermined region. The emittance was then calculated using the Stefan-Boltzmann Law and the assumption that the power was dissipated solely by thermal radiation. An oxidized stainless steel specimen of known emittance was used for verification.

For the virgin (unoxidized) specimen, measured emittance ranged from $0.159 \pm 1.34\%$ at 913 K to $0.200 \pm 1.25\%$ at 1091 K. The highest emittance value obtained was $0.339 \pm 1.63\%$ at 1269 K for the specimen after visible surface oxidation was noted. The available vacuum was found to be inadequate for preventing oxidation of the heated Nb-1% Zr, causing a steady increase in the emittance value of the specimen from one experiment run to the next.

TOTAL HEMISPHERICAL EMITTANCE OF NIOBIUM-1% ZIRCONIUM FUEL CLADDING FOR THE SP-100 SPACE REACTOR

I. Introduction

Background

The SP-100 Program, as described by J. Angelo and D. Buden in Space Nuclear Power, is a venture begun in 1983 by the Department of Defense, the Department of Energy, and the National Aeronautics and Space Administration to "jointly develop space reactor technology" (3:232). Goals for the program include a net electric power output of 100 kW, a mass constraint of 3,000 kg, a maximum length of 6.1 m, and safe operation (3:233). Throughout the entire project, the design guidelines have included a requirement for ensuring full consideration of aerospace nuclear safety. This study concerns one safety aspect: the question of how well the Nb-1% Zr cladding can radiate decay heat from the core following the loss of its primary coolant.

The coolant, liquid lithium, circulates under pressure around the fuel pins (uranium nitride pellets clad in tubular sleeves of Nb-1% Zr) (3:234). Normally, the coolant leaves the reactor core at temperatures between 1131 K and 1375 K (8:1). Since a space environment subjects the reactor to bombardment by meteors and orbiting space debris, the cooling system is vulnerable to puncture. Such an event would evacuate the space around the pins and is known as a

"loss-of-coolant accident" or LOCA. Without the presence of the coolant, the danger exists that the maximum core temperature of 2000 K could be exceeded (4:575).

Following a LOCA and an emergency reactor shut down, the core must survive the heat accumulating from decaying fission products. In order to control the temperature of the core and prevent structural failure, the decay heat, initially produced at the rate of about seven percent full power, would need to be removed. One solution uses an auxiliary supply of lithium that is isolated from the primary reservoir and connected to tubes interspersed among the fuel pins. For maximum effectiveness, these tubes, called cold fingers or bayonets, would be arranged within the core so that each can dispose of heat from several nearby fuel pins. In addition, no pin must be allowed to exceed the 2000 K temperature limit.

Robbins (14) used T. Kao's Thermal System Analysis Program (TSAP) code (10), in modeling the proper placement of the bayonets, based on assumed values of emittance. The important trend demonstrated by TSAP is that higher emittance values for the fuel cladding corresponded to a relatively larger zone of influence for any one bayonet. It was thus shown that the total number of required bayonets decreased as the emittance increased.

Definition of Emittance

Emittance, often called thermal emittance, is the property of a material that relates the amount of energy radiated to that of a black body emitter at the same temperature. A point of possible confusion exists in that emittance is often used interchangeably with "emissivity". However, one system of nomenclature in use reserves the "ivity" suffix to intensive properties describing a material in general. Extensive properties, such as emittance, would be used to describe a specimen of the material (7:3-4). For instance, emissivity would apply to the alloy Nb-1% Zr, while emittance might be used in describing the surface of a 12-inch-long, thin-walled, hollow cylinder of polished Nb-1% Zr.

According to the Standard Test Method for Total Hemispherical Emittance of Surfaces from 20 to 1400 °C, set forth by the American Society for Testing and Materials (ASTM C 835-82, Reapproved 1988), emittance can be characterized into normal vs hemispherical and spectral vs total. Normal emittance corresponds to energy radiating normal from the surface, while hemispherical emittance relates to energy radiating at all angles (2:1). Some applications require characterization of the energy spectrum. In those cases, spectral emittance would be used to describe an object's radiation properties as they apply to a specific spectral band. Accordingly, total emittance would include all wavelengths. Total hemispherical emittance is used here, be-

cause the interest lies in all energy being radiated at all angles from the bare fuel pin cladding. Figure 1 shows three views of radiation from a point on the cylinder surface and demonstrates the hemispherical nature of such radiation.

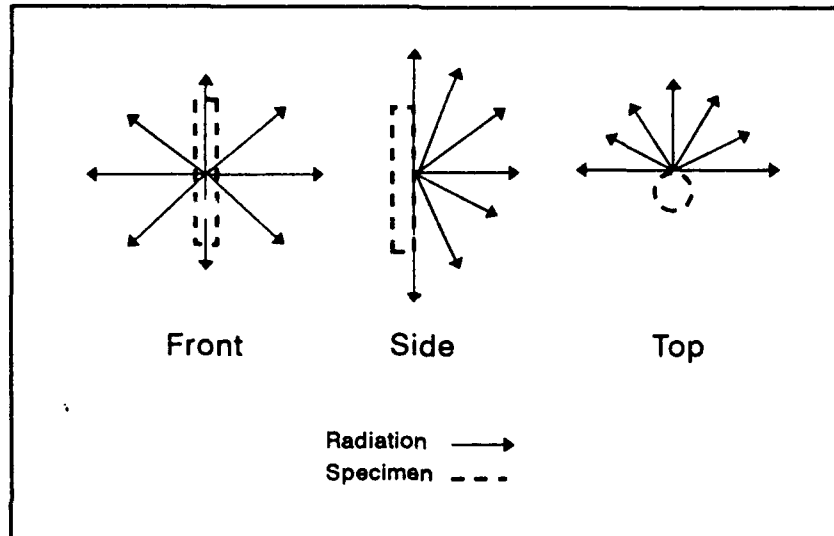


Figure 1. Hemispherical Radiation from a Point on the Surface of a Cylinder

Problem

This study is an attempt to adapt the method prescribed for thin strips by ASTM C 835-82 for use on a thin cylindrical test specimen. A working apparatus conforming to the standard was located at ORNL, and a visit was made to inspect this apparatus and the experimental procedure. Since a long, thin-walled cylinder could be considered a thin metal strip bent to form a continuous surface, it was determined that the ORNL design would work. Several assumptions

were required in order to adapt the design to this study while maintaining compliance with the ASTM standard; the assumptions are discussed separately in section I. Figure 2 shows an overview of the apparatus.

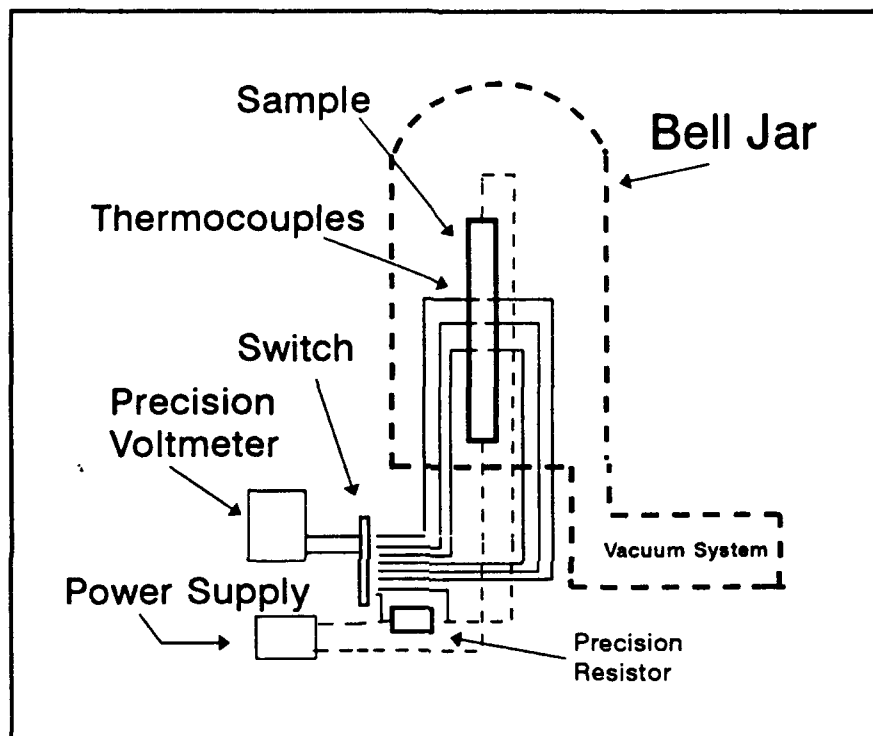


Figure 2. Overview of Apparatus

This study provides values for the total hemispherical emittance of a sample specimen of SP-100 specification cladding obtained from Los Alamos National Laboratory (LANL). The sample was approximately 30 cm long with an outside diameter of 0.76035 cm. Type S thermocouples were first attached to the sample. Also serving as supports, copper clamps were used inside the bell jar to connect power

lines from the DC source to the sample. The clamps and cables were required to be large enough to handle currents up to 180 amps for heating the sample.

In order to obtain a value for emittance, the voltage drop across a predetermined section of the sample was measured, along with the current flowing through the sample and its surface temperature. A discussion appears in Section II concerning how these physical values were used in calculating emittance.

Scope

Senor and others correlated existing data sets and demonstrated a temperature dependence for total hemispherical emittance of the subject alloy (15:206). Ideally, this dependence should be characterized for cladding surface temperatures up to 2000 K, the upper operating limit for the SP-100 core. However, this study limited the temperature to 1268 K maximum due to power supply constraints. The apparatus initially included a 75 amp DC power supply, replaced by a 180 A supply for the final series of measurements.

Another limiting factor was the availability of suitable vacuum equipment. To avoid convective loss, the vacuum chamber required a pressure of 1.3 mPa or less (2:3). Otherwise, convective loss would drive down the surface temperature and increase the apparent emittance. In addition, the vacuum prescribed by the ASTM standard was insufficient for Nb-1% Zr, which exhibited surface oxidation

problems at pressures as low as 0.53 mPa. The steady oxidation of the sample gradually increased the emittance over time.

Assumptions

The derivation used in this method to calculate emittance required the consideration of several basic assumptions. The first three were based on the ASTM standard. They are:

1. The enclosure is a blackbody emitter/absorber at a uniform temperature. The ASTM standard permits the use of an uncoated glass bell jar because "it absorbs or transmits most of the incident infrared radiation" (2:9).
2. The sample's total hemispherical emittance equals its absorptance. This assumption refers to the exchange of diffuse blackbody radiation between the sample and its surroundings.
3. There is no heat loss from the test section by convection or conduction (2:2).

Section II contains a discussion of these assumptions in greater detail, as well as a fourth assumption required due to the geometry involved.

4. The dimensions of the cylindrical specimen are sufficient to prevent more than a negligible net gain or loss of radiative energy at the inner surface of the test section.

Approach

To establish a basis for this study, Section II will begin with the development of the theory involved in emittance measurement. A brief introduction explains the relevance of emittance to radiative heat transfer. Following the introduction, all relevant heat transfer mechanisms are applied to the problem.

Following the theory, Section III covers the design and construction of the apparatus. The assumptions made earlier will be treated in greater detail to explain how they affected the design. Section IV explains the experimental procedure. Included in this section are the procedures for operating the apparatus and for gathering data. The effect of design constraints on data collection will be discussed.

Section V contains the results of the study, along with an error analysis and the conclusions reached. Included in this section is a comparison of the AFIT results with those from ORNL for the ORNL oxidized stainless steel emittance standard. The Nb-1% Zr results are compared with Senor's correlation mentioned earlier. Finally, Section VI summarizes the conclusions made and contains recommendations for further research on Nb-1% Zr fuel cladding emittance.

II. Theory

Introduction

This section contains the theory underlying the assumptions made when measuring total hemispherical emittance. First, the Stefan-Boltzmann Law will be used to highlight the difference between a blackbody radiator and less-than-ideal radiators, reemphasizing the relevance of thermal radiation to the study. Next, the heat transfer mechanisms present in a generic emittance laboratory experiment will be discussed as a basis for the method used. Finally, the theory will be adapted to the particular case at hand, a hollow cylindrical radiator of a refractory alloy.

Stefan-Boltzmann Law

The Stefan-Boltzmann Law states that the power per unit area radiated by a "blackbody" or ideal radiator is proportional to the fourth power of its absolute surface temperature. This relationship is given by

$$P_a = \sigma T^4 \quad (1)$$

where

P_a = power radiated per unit area
 σ = Stefan-Boltzmann Constant
 T = absolute temperature

To account for the loss of radiation efficiency when the radiator is less than ideal, one uses a factor known as emittance, or the ratio of the power per unit area radiated

by the non-blackbody to that radiated by a blackbody at the same temperature. Eq (1) thus becomes

$$P_a = \epsilon \sigma T^4 \quad (2)$$

where ϵ is the emittance, a positive number less than one for all non-ideal radiators.

Now that the background has been established, the remainder of Section II will be used to derive the relationships used in this study.

Heat Flow in a Solid Cylinder of Conducting Metal

Consider a solid, conducting metallic cylinder with DC current applied to the ends via electrodes. Due to its own resistivity, the cylinder will begin to produce thermal energy, and several heat transfer processes will attempt to return the cylinder and its surroundings to thermal equilibrium. Besides radiation, these processes include conduction, convection, absorption, and the storage of internal energy (1:294).

A simple expression for the transport processes mentioned above per unit length is

$$P_D = P_R - P_a + P_{cd} + P_{cv} + P_s \quad (3)$$

where

P_D = electric power dissipated per unit length
 P_R = power radiated away per unit length
 P_a = power absorbed from surroundings per unit length
 P_{Cd} = power lost through conduction per unit length
 P_{Cv} = power lost through convection per unit length
 P_s = power lost to internal energy per unit length

These terms shall be treated one at a time in the general case of the solid cylinder, followed by an adaption to the specific case of the hollow cylindrical cladding.

First, the rate of increase in internal energy stored in the cylinder shall be examined. This heat transfer mechanism is given as

$$P_s = DAC \frac{dT}{dt} \quad (4)$$

where

P_s = power stored per unit length in $W\ m^{-1}$
 D = density in $kg\ m^{-3}$
 A = cross sectional area in m^2
 c = specific heat in $J\ kg^{-1}\ K^{-1}$
 T = absolute temperature in K
 t = time

In order for this term to have any effect, the temperature must be changing with respect to time. At this point, a boundary condition shall be imposed on the problem: the derivative of temperature with respect to time must be 0, or in other words, a steady-state condition must be present. Thus, the P_s term is eliminated.

The next term to be discussed shall be the conduction loss term. In order for heat conduction to occur, a temperature gradient must exist. Therefore, if it can be shown

that no temperature gradient exists along a given coordinate, it can be said that the conduction loss term contains no component associated with that coordinate. To assume that no net conduction loss occurs from a particular zone of interest in a cylindrical coordinate system, then, one must show that no temperature gradient exists along the radial, azimuthal, or axial coordinates. The following section contains a treatment of this problem as it applies to the specimen used in emittance measurement.

Ordinarily, one might use LaPlace's equation to describe the steady-state temperature distribution in a cylinder. In cylindrical coordinates, it is given as

$$\nabla^2 T = \frac{1}{\rho} \frac{\partial}{\partial \rho} \left(\rho \frac{\partial T}{\partial \rho} \right) + \frac{1}{\rho^2} \frac{\partial^2 T}{\partial \theta^2} + \frac{\partial^2 T}{\partial z^2} = 0 \quad (5)$$

where ρ , θ , and z are the radial, angular, and longitudinal coordinates respectively. The basic solutions of interest for T are

$$T = \left\{ \begin{array}{l} J_n(k\rho) \sin(n\theta) \exp(-kz) , \\ J_n(k\rho) \cos(n\theta) \exp(-kz) \end{array} \right\} \quad (6)$$

where k (real) is a zero of the Bessel function J_n and the separation constant n is an integer. However, for the purposes of this study, the dimensions and location of the zone of interest will be chosen such that the temperature within the zone has no dependence on ρ , θ , or z .

Heat Flow in a Thin, Hollow Cylinder of Conducting Metal

Consider a 30 cm long section of SP-100 fuel cladding, a thin-walled hollow cylinder with (1) a wall thickness very small in relation to the cylinder's diameter and length, and (2) a diameter very small in relation to the cylinder's length.

The discussion will begin with heat conduction in the radial direction. The analogy to the ASTM emittance calculation standard is the heat transfer through the thickness of the flat metal strip. The ASTM standard assumes a sample thickness too insignificant to allow a temperature gradient to exist between the two flat sides, implying no heat conduction normal to the plane of the specimen. In other words, all heat is considered to be generated on the two flat surfaces of the strip. Taking a similar approach with the cylindrical specimen, one can assume a wall thickness such that all heat is generated on the inner and outer surfaces with no temperature gradient between them.

Next, the angular component of heat conduction will be examined. If one assumes that the cylinder is homogeneous and uniform, there is no basis for a temperature gradient to exist as a function of θ . Thus, no angular component of heat conduction exists.

Now that the radial and angular dependencies of the temperature have been eliminated, only the question of a longitudinal dependence remains. At this point, an assumption is made that the cylinder is very long in relation to

its diameter. By measuring the surface temperature of the cylinder, one can find a region (Figure 3) near the middle such that the axial temperature gradient (caused by conduction out the electrodes) is essentially zero (2:9). The zone of interest, or test zone, for this study shall be chosen so that its boundaries are within this region lacking an axial temperature gradient.

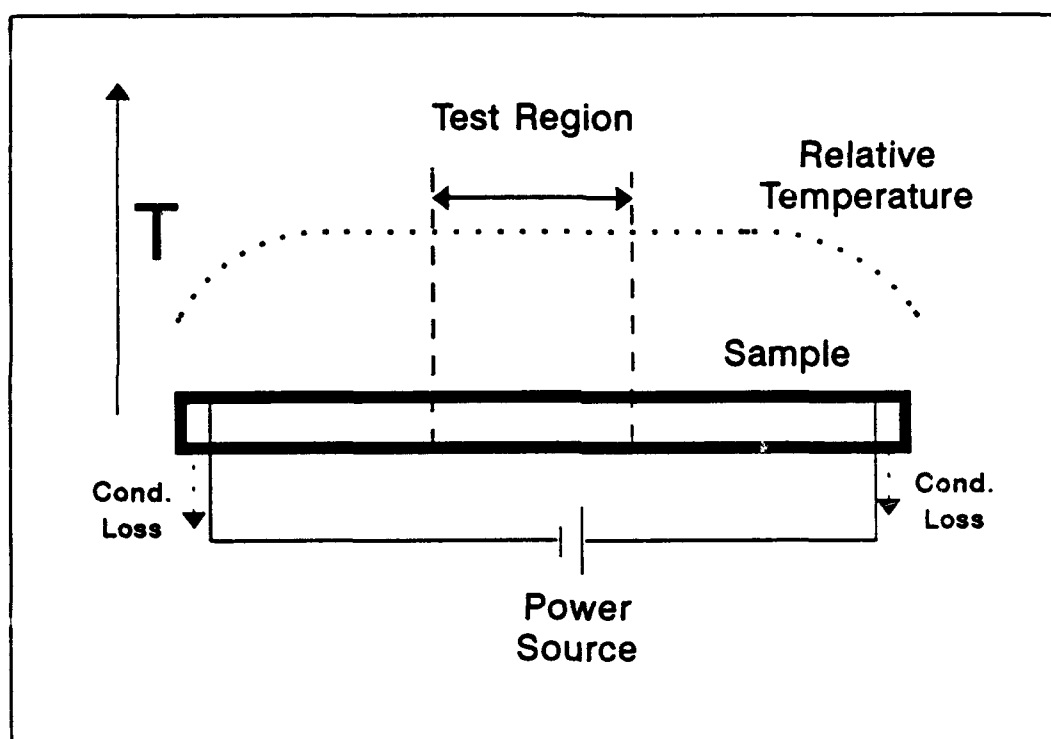


Figure 3. Axial Temperature Distribution Along an Electrically Heated Metallic Cylinder

Since it has been shown that no temperature gradient exists across the boundaries of the test zone, it can therefore be said that there can be no net heat conduction loss from the zone. Thus, the P_{cd} term in Eq (3) is eliminated.

Before moving on to convective loss, it is appropriate to mention the heat conductive loss caused by attaching thermocouples to the sample within the test zone. Such loss creates a temperature depression at the weld. Since thermocouple wires of 0.003" diameter are welded to the specimen's surface in the zone of interest, any conduction loss out these wires would lower the actual surface temperature in the weld region. Using the ASTM standard, it is assumed that any loss through such small diameter wire would be negligible. In fact, the ASTM standard states that "the heat conducted out through the thermocouple leads is usually neglected" (2:9).

Next, the convection term P_{cv} in Eq (3) shall be considered. Since the study attempted to simulate a space environment, a vacuum bell jar was used. The convection heat transfer coefficient is zero in a vacuum, immediately eliminating the convection term.

Eq (3) has now been reduced to

$$P_D = P_R - P_A \quad (7)$$

P_R , the power radiated per unit length, can be expressed as

$$P_R = \epsilon_H A_L \sigma T^4 \quad (8)$$

where

ϵ_H = total hemispherical emittance
 A_L = radiating area per unit length of specimen

A reciprocal heat transfer process occurs, wherein the radiator can absorb heat from its surroundings, assumed here as a black body absorber/radiator. This process is given by

$$P_A = \alpha_H A_L \sigma T_0^4 \quad (9)$$

where

P_A = power absorbed per unit length of specimen
 α_H = total hemispherical absorptance of the specimen
 T_0 = absolute temperature of the surroundings, including the jar and the ambient air

The electric power dissipated per unit length, P_D , is simply the current flowing through the specimen times the voltage drop per unit specimen length.

Substituting Eqs (8) and (9) into Eq (7) yields

$$P_D = \epsilon_H A_L \sigma T^4 - \alpha_H A_L \sigma T_0^4 \quad (10)$$

By multiplying the equation through by unit length and dividing through by σA , one obtains the relationship

$$P_D = A \sigma (\epsilon_H T^4 - \alpha_H T_0^4) \quad (11)$$

Eq (11) relates the radiative heat transfer into and out of a specified area with the electric power dissipated within that area. The right side can be regrouped to obtain

$$P_D = \epsilon_H A \sigma \left(T^4 - \frac{\alpha_H}{\epsilon_H} T_0^4 \right) \quad (12)$$

According to Abbott, the term in Eq (12) containing T_0 is often ignored, accounting for an error of less than 1% when T is at least 3 times T_0 (1:295). Attempted here initially, the approximation introduced errors of up to 3% in this study, and was abandoned. The ASTM standard allows the use of an uncoated glass bell jar by assuming that the energy incident on the bell jar is mostly either absorbed or transmitted. Therefore, T_0 was assumed to be the ambient air temperature of 295 K. In addition, the ratio of absorption to emittance was deemed unity by assumption 2 on page 7. Solving for ϵ_H , then, gives

$$\epsilon_H = \frac{P_D}{A\sigma(T^4 - T_0^4)} \quad (13)$$

the expression used to calculate total hemispherical emittance in this study.

One final assumption was made concerning radiation. As stated above, the cylinder was assumed to have a small diameter relative to its length. The purpose for this was to eliminate net radiation gain or loss at the zone of interest's inside surface. It is therefore assumed that a narrow, long, hollow cylinder would facilitate a condition of local thermodynamic equilibrium inside the tube away from the ends. See the recommendations section for comments concerning this aspect of the problem.

III. Apparatus

The Basics

As shown in Figure 1, the apparatus for measuring total hemispherical emittance was comprised of a vacuum system, bell jar, DC power supply, specimen holder, precision voltmeter, thermocouples, and temperature reference bath. A multiposition switch box allowed data to be taken without disturbing any leads or connections.

Vacuum System

A six-inch water-cooled diffusion pump was used in the vacuum system, backed by a mechanical roughing pump. To begin with, two problems associated with this system had to be solved. First, to prevent contamination of the bell jar and contents from any backstreaming pump oil, a cold trap was used. It was maintained at around -8° C using a standard refrigerator compressor and R-12 coolant. The cold trap added its own problem: an insufficient load to the compressor to prevent freezing of the coolant return line. Electrical heat tape was applied to the line to prevent freezing.

An ionization gauge was used for monitoring the vacuum in the bell jar. It could be isolated from the pumping system, as required, to perform static pressure checks.

Bell Jar

A quartz bell jar with a wall thickness of one-eighth inch was used to house the specimen. For safety reasons, a protective metal screen was installed on the outside, surrounding the jar. The inner walls were not coated, and no water cooling was employed.

The requirement to keep the recommended 100 K difference between the bell jar and the specimen was accomplished at ORNL by using a water-cooled, coated metallic bell jar (2:2). It approximated a blackbody absorber/radiator when exposed to the heated samples. On the other hand, the quartz bell jar used in this study used no external cooling. It was assumed that the high energy radiation from the sample was either transmitted through the bell jar to the surrounding room or absorbed by the jar (2:9). Other high energy sources (i.e. open flames, sunlight) were not allowed to be present during experiment runs. Finally, the sample was mounted off-center in order to preclude a focusing effect from the minimal reflections of high-energy radiation from the bell jar wall (2:9).

DC Power Supply

Two different Intermagnetics DC power supplies were used. Both were designed for high-current, low-voltage electromagnet applications. Rated at 75 amperes maximum, the first supply proved insufficient for heating the Nb-1% Zr sample appreciably due to the relatively low resistivity

of Nb-1% Zr. Therefore, the first supply was replaced with one rated at 180 A maximum. Each contained a precision resistor in series with one pole of the output lines. Measuring the voltage drop across the resistor permitted calculation of current at up to six decimal places of precision. Since the resistor in each supply was calibrated to provide a drop of 100 mV at full rated current, a precision digital voltmeter was used as a handy current meter by displaying the percentage of maximum current (either 75 A or 180 A) flowing through the specimen.

Due to the relatively high current involved, power was supplied to the specimen via large insulated copper cables of 00 gauge. For reasons explained in Section IV, the experimental procedure required a reversal of current during measurements at each data point. Since reversing these large cables took enough time to allow the temperature of the sample to fall, it was determined that mechanical switching would be preferable. Using available copper stock, the AFIT Model Shop fabricated a double-pole, double-throw knife switch for this purpose. The knife switch was wired into the circuit so that it reversed the polarity when thrown. In order to ease the strain of sudden open circuit conditions on the low-impedance power supplies during polarity reversal, a copper shorting bar was used.

Precision Voltmeter

A Hewlett Packard Model 3478A Multimeter with six digit display was used for taking thermocouple emf, specimen voltage drop, and precision resistor voltage drop measurements. Twenty times more sensitive than required by ASTM C 835, the meter had a sensitivity of 0.1 μ V. Although not exploited due to time constraints, the meter possessed a digital data output capability for automatic data recording.

Specimen Holder

As previously noted, the specimen was mounted off-center to minimize the impact of normal reflections from the bell jar wall. Supporting the ends of the specimen were two clamps fashioned from woven copper braid, flexible enough to allow for specimen expansion during increasing temperature. These clamps were also attached to standard laboratory clamp stands and to the power supply cables. As shown in Figure 4, the clamp stands also served to support the thermocouple leads, separating them from the specimen and from each other.

Thermocouples

Also referred to as Type S, platinum/platinum-10% rhodium thermocouples were chosen for this study primarily for the temperature range they span, but also because of their ductility. Suitable positions for mounting thermocouples were scored on the specimen with a scalpel, and the distance between them was measured under a microscope.



Figure 4. Nb-1% Zr Specimen Mounted Inside Bell Jar

Short (few cm) lengths of 3 mil gauge thermocouple stock were spot welded to the marked positions using a resistance welder at the EG&G Mound Technologies, Inc. Facility. A total of three Pt, Pt-10% Rh thermocouple pairs were attached at approximately 4 mm intervals. Figure 5 shows the relative placement of the thermocouples and power electrodes.

Laser welding was attempted but was abandoned due to the degree of difficulty involved in working with niobium. Instead, resistance welds using copper needles proved much more effective. In order to preclude the occurrence of oxidation during the procedure, a procedure developed at Mound was employed involving the direction of argon through a diffuser stone at the weld at a flow rate of 6 cubic feet per hour (9).

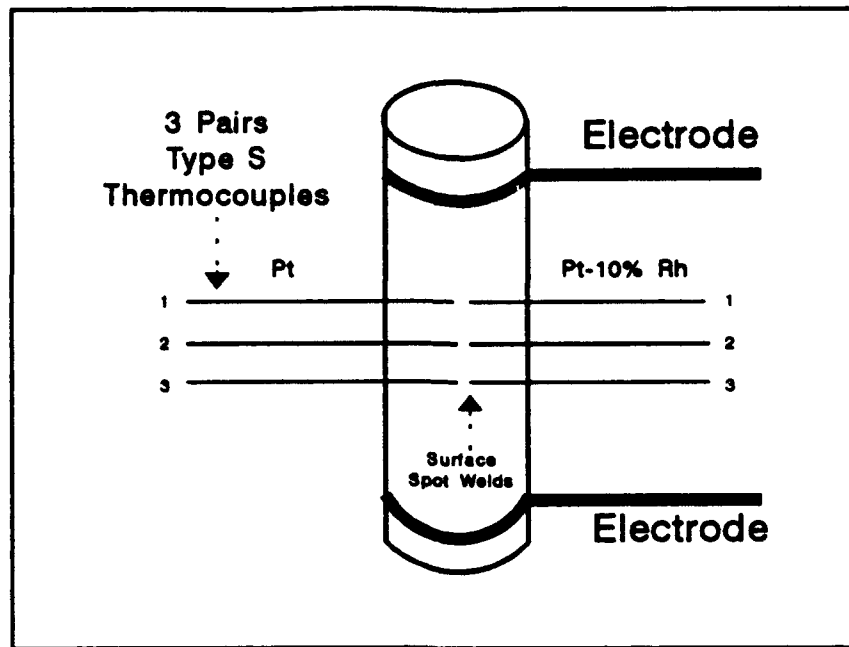


Figure 5. Thermocouple and Electrode Placement

Although Pt, Pt-10% Rh thermocouples have response curves published up to 1938 K, a eutectic forms at the weld between Pt and Zr, with a melting point of 1458 K. Exceeding 1458 K could in weld failure (11). Other eutectics exists between Nb and Pt, Nb and Rh, Zr and Rh, etc., but the lowest melting point is that of Pt and Zr. For that reason, three pairs of tungsten-26% rhenium, tungsten-5% rhenium thermocouples were also welded to the specimen in an alternating arrangement in anticipation of being able to continue taking data at temperatures beyond the melting point of the Pt-Zr eutectic. As it turned out, the higher temperature range was not explored due to power supply constraints, so the tungsten-rhenium thermocouple stubs were not used.

At this point it is necessary to mention that the apparatus was constructed using cold-worked thermocouple material which was not annealed prior to use. Hindsight suggests a more proper technique of annealing the thermocouple wire stock prior to building the feed through assemblies or welding the pigtails onto the sample. In addition, the only thermocouple calibration attempt was made at the ice point. Again, a more prudent procedure would probably have included some method of obtaining a calibration point at high temperature. Both these problems are discussed in the results.

A thermocouple feed-through and extension assembly was fabricated by the AFIT Model Shop using a plexiglass flange, high-vacuum epoxy, and 10 mil gauge Pt, Pt-10% Rh thermocouple wire. After installing the assembly into a port on the bell jar support table, the 10 mil leads were threaded into short lengths of ceramic insulation and were resistance welded to the 3 mil pigtails protruding from the specimen. Once again, argon was used to provide an inert welding environment. The welds between the two gauges of wire were then cleaned with nitric acid to remove any contamination acquired during assembly.

An aluminum-walled insulated ice bath was fabricated by the AFIT Model Shop for use as a thermocouple temperature reference. (The ice bath was necessary due to the fact that the published thermocouple response tables were based on a reference temperature of 0° C.) Holes were drilled into the

lid into which rubber-stoppered glass tubes were inserted. Each tube was filled with a small amount of mercury into which a single thermocouple lead, connected to its copper extension wire, was inserted. The copper extension wires were routed through a multi-position push-button switch to the voltmeter. For ease in taking measurements, the switch was wired so that each of the three thermocouples could be independently selected. Figure 6 depicts the wiring arrangement for measuring the voltage produced by thermocouple number 1--the switch and all other wires are omitted from the drawing for the sake of clarity.

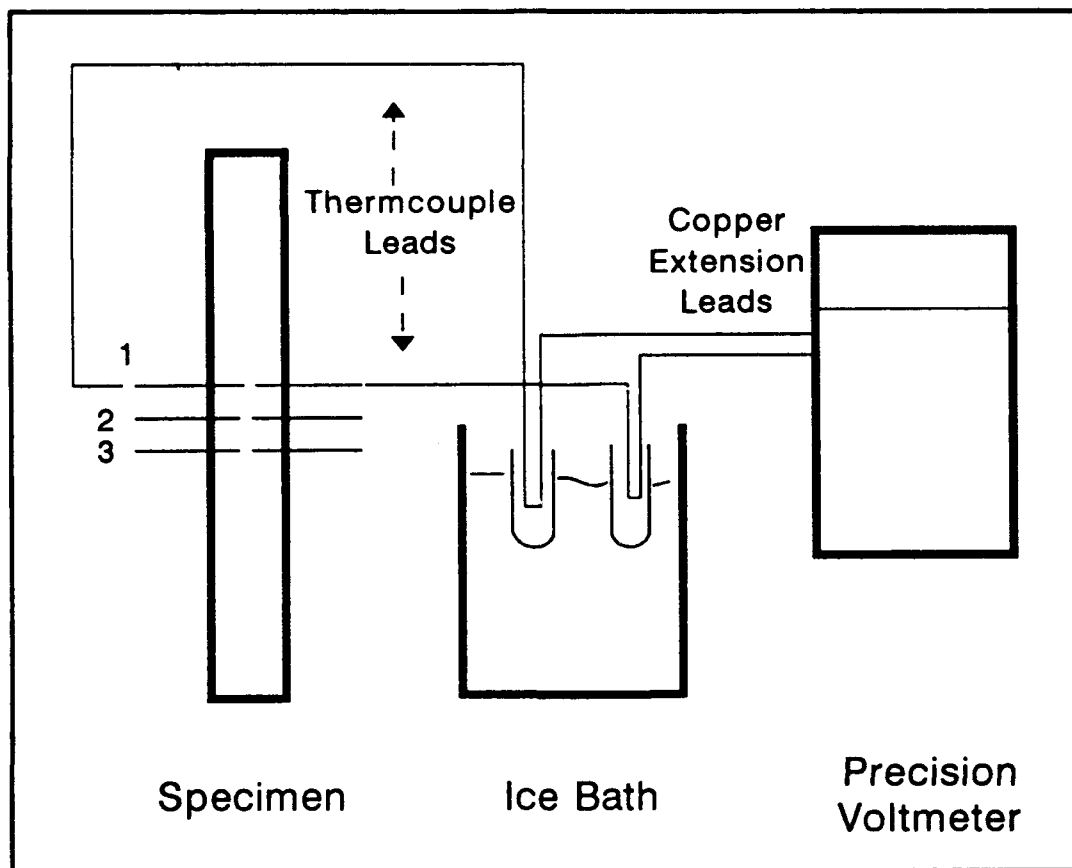


Figure 6. Wiring Diagram for Thermocouple Number 1.

In addition, two other positions on the switch allowed for voltage drop measurements across the sample between the top (number 1) and middle (number 2) junctions and between the middle and bottom (number 3) junctions respectively. This function of the apparatus is demonstrated in Figure 7 for the top two thermocouples. Again, only the active circuit is depicted.

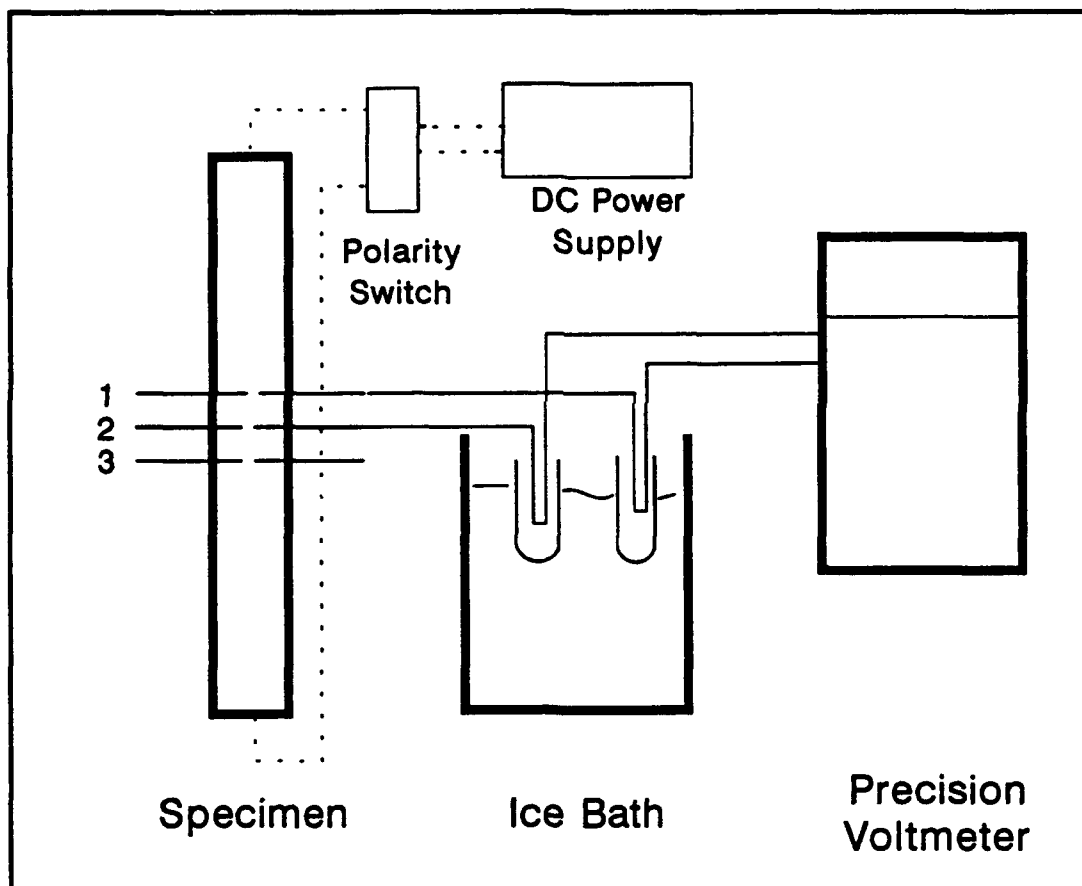


Figure 7. Wiring Diagram for Measuring Voltage Drop Across Specimen Between Thermocouples 1 and 2

Finally, a switch position was reserved for measuring the voltage drop across the power supply's precision resistor, shown in Figure 8. Thus, acquiring data at each point

was relatively simple--the operator had only to record the voltmeter readout corresponding to each button on the switch.

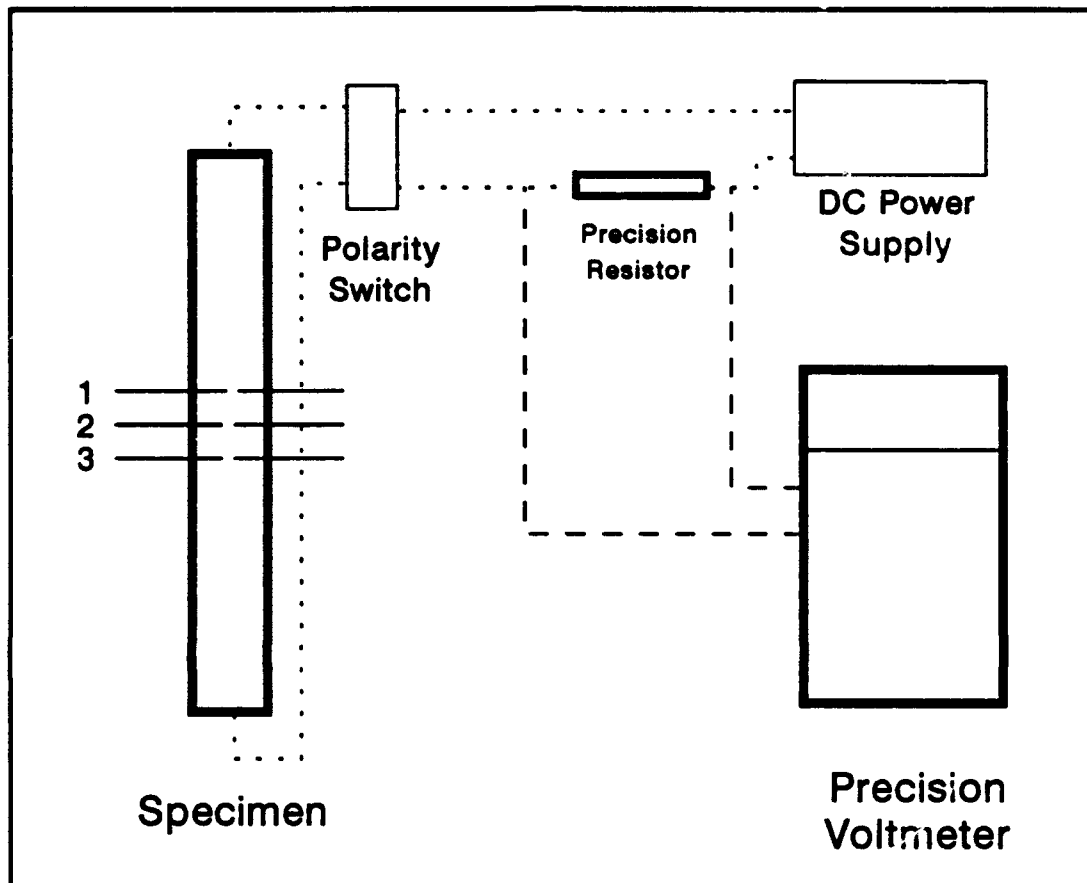


Figure 8. Wiring Diagram for Measuring Voltage Drop Across Precision Resistor

IV. Experimental Procedure

Preparation

The apparatus was first operated using a thin, flat specimen of oxidized stainless steel (SS) obtained from D. McElroy, ORNL. The strip was approximately 20 cm long, 1.25 cm wide and 0.05 cm thick. It came prepared with three pairs of Pt, Pt-10% Rh thermocouples spot welded in a row near the center of one side about 2 cm apart. Configured essentially the same as the Nb-1% Zr sample, the SS specimen was used to verify the experimental procedure. The value for the emittance of this specimen had been previously measured at ORNL using an apparatus conforming to ASTM Standard C 835. The dimensions for computing surface areas between thermocouple junctions for both the SS and the Nb-1% Zr specimens had been previously measured under a microscope to five significant digits and entered into the notebook.

Following the data collection runs with the SS specimen, the apparatus was reconfigured for the Nb-1% Zr tube. The thermocouple extensions required rewelding to the Nb-1% Zr specimen's thermocouple pigtails and the electrodes had to be reconfigured to accommodate the change to a cylindrical geometry. The procedure for taking data was essentially the same for both specimens.

Before each data collection run was made, the ice bath was prepared using a mixture of de-ionized water and cracked ice made from the same water. While waiting for the temper-

ature of the bath to stabilize at the freezing point, the following pre-check items were accomplished. First, a visual inspection was performed of all electrical connections and a continuity check made of each thermocouple lead. Next, the vacuum gauge reading was recorded. For safety concerns, the bell jar was then inspected for surface cracks which might indicate imminent failure of the quartz under uneven heating conditions. The power supply and voltmeter were turned on and allowed to warm up. Finally, when all checks were complete, the power supply was ramped up slowly to allow a check of the thermocouples and the voltmeter. At this point, an arbitrary determination was made whether to begin taking data at maximum temperature and work down the scale or vice-versa. Power was then advanced to the starting point, and the system was left in this configuration until the temperature stabilized. Stabilization was determined to be reached when no change occurred in measurements of thermocouple emf over a 2 minute interval.

Data Collection

When temperature stabilization was reached, the system was considered to exist in a state of thermodynamic equilibrium. A check of the ice bath was then made to ensure the proper reference temperature was available for the thermocouples. Data collection began by entering the following data into the notebook:

1. Time of Day
2. Polarity (forward or reverse)
3. Current as percent of maximum, read directly from voltmeter (See section III.)
4. Emf measured from thermocouple 1 in V
5. Emf measured from thermocouple 2 in V
6. Emf measured from thermocouple 3 in V
7. Voltage drop between thermocouples 1 and 2 in mV
8. Voltage drop between thermocouples 2 and 3 in mV

Following collection of the above data, the power supply was short-circuited and the knife switch thrown to the opposite position in order to reverse the polarity of the current applied to the specimen. As soon as the switch was thrown, the shorting bar was removed. An explanation for the polarity reversal and the short circuit procedure follows.

The purpose for reversing polarity was to provide another emf measurement to counteract bias error introduced by slightly misaligned thermocouple wires. The mean of the two opposite-polarity measurements was taken and used as the "true" emf at the junction. Each reversal was accomplished after first shorting out the low-impedance power supply to protect it from frequent full-load to open-circuit transitions and vice versa.

When polarity reversal was accomplished, the sample was allowed to return to equilibrium, determined by noting a steady temperature. Then, the data collection procedure was

repeated, except for the polarity reversal. Thus ended the collection at the initial specimen temperature.

Next, the power supply was adjusted either up or down, as required, by a predetermined amount. The polarity used in the last half of the prior collection run was used in order to reduce by half the number of power interruptions to the sample. After allowing the system to reach equilibrium, another set of data was taken. Then the polarity was reversed, and the process repeated until the predetermined ending point was reached.

At various intervals during the procedure, the temperature of the ice bath was checked, and ice was added as necessary. Bell jar pressure was continually monitored.

See Appendix B for sample data. Table III shows sample data using the oxidized SS specimen, and Table IV shows the data for the Nb-1% Zr specimen before visible oxidation set in.

Data Reduction

National Bureau of Standards (NBS) Circular 125 was consulted to obtain thermocouple response curves (17). The reference listed emf potentials for Pt, Pt-10% Rh thermocouples as an expanded power series in temperature (See Appendix A). An iterative solution was necessary to calculate temperatures from emf data measurements. For this effort, TK Solver Plus, Academic Edition, was employed (16).

Once the temperatures were obtained, the mean temperature was calculated for each pair of values obtained from thermocouples 1 and 2, and used to represent the temperature of the zone between the two thermocouples, designated the top zone. Likewise, the temperature for the bottom zone was obtained by averaging those from thermocouples 2 and 3.

Next, the voltage drop between thermocouples 1 and 2 was multiplied by the current flowing through the sample to obtain the amount of electric power being dissipated within the top zone. Likewise, the power for the bottom zone was calculated using thermocouples 2 and 3. The power, temperature, and surface area (previously measured) were entered into Eq (13) to obtain the emittance. This was done for both the stainless steel and the Nb-1% Zr specimens. During the error analysis, it was determined that T_0 could not be ignored. T_0 was assumed to be 295 K for all data points.

V. Results

Introduction

This section contains an analysis of the results of the emittance measurements and a treatment of the associated errors. Results for the stainless steel emittance standard are presented first, followed by the results for the fuel cladding specimen. The method used for estimating the error in the reported emittance values is taken from ASTM C 835 standard and is shown in Appendix C.

SS Specimen Emittance Values

Emittance measurements were made of the SS strip in this study from about 780 K up to about 945 K. See Appendix B, Table V for a sample of initial calculation results. Figure 9 shows an initial comparison between the results of this method and those from R. S. Graves and D. McElroy of

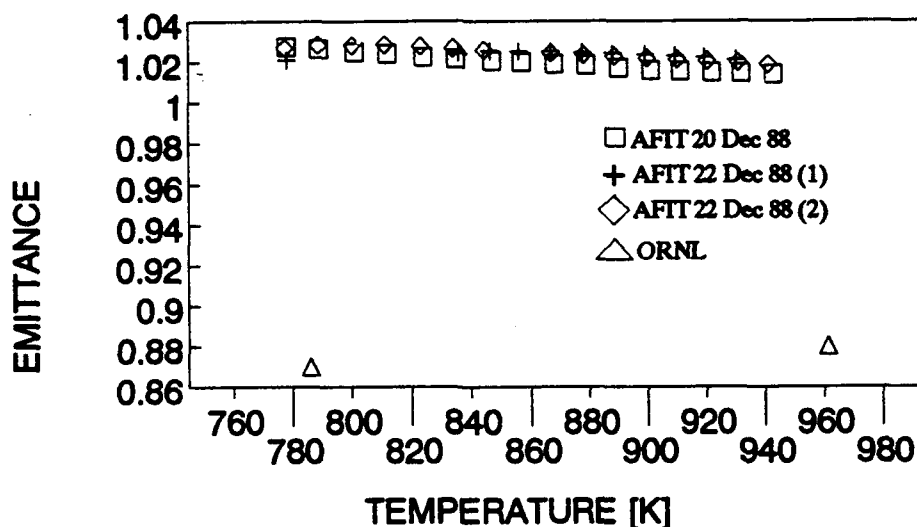


Figure 9. Initial Results Compared to ORNL, Emittance vs Temperature, SS Specimen

ORNL (6). This study yielded an initial value for the emittance of about 1.02 at 900 K as compared to a linearly interpolated value of 0.88 for the ORNL data. A linear interpolation for the ORNL data was determined to be appropriate in this case due to the availability of only two data points.

At this point, it was apparent that the thermocouple calibration error of -34.8 K at room temperature was prevalent at higher temperatures and could not be ignored. Without a high temperature calibration point, it was assumed that the thermocouples responded similarly throughout the entire temperature range used. A calibration at a high temperature was not performed due to equipment and time constraints. At one point, an optical pyrometer was used to examine the surface of the heated specimen. Although the pyrometer was useful for examining the relative temperature along the surface of the specimen, no actual temperature calibration was possible due to the following reasons. First, the emittance of the object being observed was an input parameter for the pyrometer control panel, and emittance was the unknown quantity being measured. Second, the absorption characteristics for the bell jar were unknown for the spectral band at which the pyrometer was most sensitive.

In conclusion, calibration error was removed from the data by adding 34.8 K to all temperatures. Figure 10 shows one data set from Figure 9 after applying the error correction. The set, designated "AFIT 22 Dec 88 (2)" corresponds

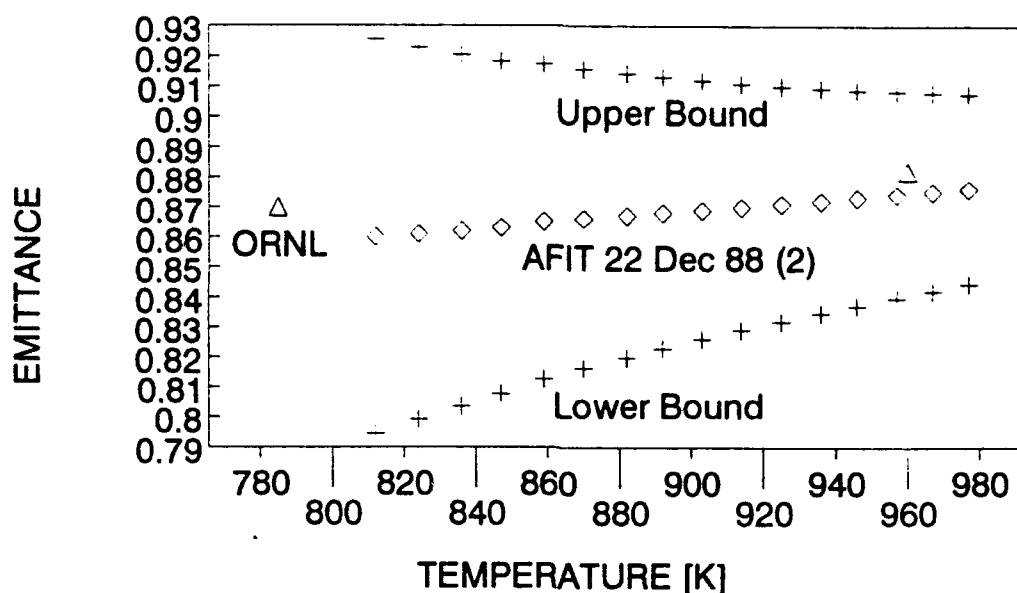


Figure 10. SS Specimen Emittance Corrected for Thermocouple Calibration Error

to Table V for Figure 9 and Table VI for Figure 10. Note that Figure 10 also includes error bars; the sources for error are discussed in the following section.

SS Specimen Error Analysis

According to T. G. Kollie and R. S. Graves, cold worked Type S thermocouples can introduce a maximum error of -8 K (12). As time passed during experiment runs, the ends of the thermocouples nearest the specimen annealed, decreasing this error by some unknown function of time, temperature, and proximity to the specimen. However, this error was part of the calibration error mentioned earlier. No separate treatment was therefore required.

The temperatures obtained from the three thermocouples varied by about 4 K maximum at any given data point. Therefore, it was estimated that the temperatures reported were

accurate to $\pm 2\%$. The uncertainty in the emittance for the stainless steel specimen typically ranged from about $\pm 3.6\%$ to $\pm 7.6\%$ (See Appendix B, Table VI for the corrected SS calculations with estimated uncertainty.)

Nb-1% Zr Specimen Emittance Values

The first set of measurements made using the Nb-1% Zr specimen were taken to represent the "virgin" (unoxidized) condition. The values ranged from $0.159 \pm 1.34\%$ at 913 K to $0.200 \pm 1.25\%$ at 1091 K. The specimen underwent a steady, visible increase in surface oxidation from one run to the next, increasing the emittance in the process. The highest value recorded was $0.339 \pm 1.63\%$ at 1269 K. Figure 11 demonstrates the upward trend, and compares the results with a correlation made by Senor and others of three existing data sets (15:206).

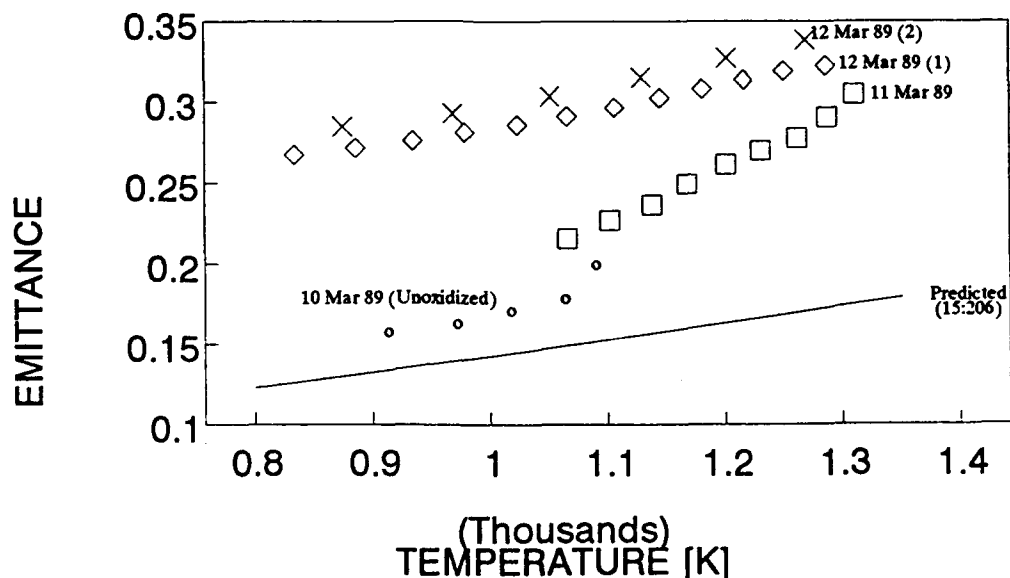


Figure 11. Emittance vs Temperature--Nb-1% Zr

The correlation was used as a "predicted" value for this study and is labeled as such in Figure 11. Appendix A, Table II contains the formula for the correlation--a third degree power series expansion in temperature. It should be noted that the surface characteristics of the specimens from which the correlated data were taken were known to be smooth. Surface oxidation levels were not addressed.

See Appendix B, Table VII for sample emittance calculations and estimated uncertainty. Table VII corresponds to the data set labeled "10 Mar 89" on Figure 11.

Nb-1% Zr Specimen Error Analysis

Besides the two sources of systematic error in temperature measurement noted for the SS specimen, an additional source appeared for Nb-1% Zr. Being an alloy of refractory metal, Nb-1% Zr has a very high tendency to oxidize when heated, even at a vacuum chamber pressure specified by ASTM C 835-82. As the experiment progressed, the surface of the Nb-1% Zr sample steadily increased in oxide content, driving up the emittance as discussed earlier. Due to the increase in emittance as an unknown function of time, temperature, and a combination of the two, an analysis of the statistical error or repeatability was not performed. The ASTM standard quotes a three-sigma bias of 5% for the method in general (2:10).

It should be noted that, although not quantified, there were several other possible sources for systematic error.

First, the assumption that the bell jar approximated a black body absorber at high specimen temperatures by transmitting the high-energy radiation might have induced additional error from reflections off the protective screen surrounding the jar. In addition, each thermocouple weld contact area might have differed enough to affect emittance calculations, despite the general guidance given in the ASTM standard.

VI. Summary and Recommendations

Summary

This study was an attempt to measure the total hemispherical emittance of a sample specimen of Nb-1% Zr fuel cladding for the SP-100 space nuclear reactor in a vacuum at operating temperatures. The purpose was to investigate the radiative efficiency of the cladding to aid in the reactor core design. Total hemispherical emittance characterizes this efficiency and affects the quantity and placement of reactor core emergency heat sinks.

Unoxidized Nb-1% Zr emittance values ranged from $0.159 \pm 1.34\%$ at 913 K to $0.200 \pm 1.25\%$ at 1091 K. The highest value obtained for the oxidized sample was $0.339 \pm 1.63\%$ at 1269 K. After initial calibration, it was discovered that a significant portion (about 25%) of the calibration error was a systematic error caused by improperly prepared thermocouples. Steady oxidation of the specimen surface affected the results, as can be seen in Figure 11.

Recommendations

The study was essentially a foundation for what was perceived as a continuing effort. Therefore, several recommendations are offered for the purpose of refining the avoidance of systematic error as well as increasing the scope of the effort to improve the applicability of the

research to the SP-100 program. A discussion of systematic error avoidance will occur first.

To begin with, any samples used in emittance measurements should have a detailed examination and appraisal of the sample's surface, to include grain size and the extent of oxidation or other surface contaminants. Preferably, this should be done by a metallurgist or someone who is knowledgeable in metallic surface features. In providing such an appraisal with the emittance experiment results, the scientific community can compare data from multiple sources in a more meaningful manner. In addition, a detailed surface appraisal would permit a meaningful comparison of laboratory emittance measurements with theoretical expressions of emissivity as a function of resistivity (1:294). For validity, such equations require the use of several assumptions about the surface conditions of the specimen.

In addition, further work on this alloy should occur only in a high-vacuum, clean-room environment. While useful for verifying the experimental procedure, the vacuum systems available for this study were not adequate to prevent surface contamination of the sample. Despite the fact that a Nb-1% Zr sample is likely to continue to outgas at high vacuum, a turbo-molecular or ion pump system would certainly be preferable to an oil diffusion pump, for instance.

Another source of error noted in this study was the use of cold-worked Type S thermocouples. Use of Type S stock should include an annealing period prior to installation in

the apparatus. In addition to annealing, the thermocouples should be calibrated at the high end of the range, and not just at the ice point. The melting point of gold (gold point) is one candidate for such a calibration; several threads of gold could be welded to the specimen near the zone of interest. As the temperature of the specimen is increased, the gold will eventually melt and fall off. At the point which this occurs, the thermocouple potential should be noted, and the calculated temperature compared to the melting temperature of gold. Of course, the characteristics of any gold-niobium and gold-zirconium eutectics must be investigated beforehand--this technique will not work if the eutectic melting point lies below the gold point. If the process could be repeated with other high melting point materials which would not contaminate the bell jar, a calibration curve could be constructed.

Yet another source of possible error was assuming no loss due to radiation from the inner surface of the test zone. Since a real fuel pin would be closed at both ends, future research should be done with closed cylinders to eliminate any possibility of radiation escaping through the holes.

Now that error avoidance has been covered, the remainder of the recommendations will be focused on improving the applicability of follow on research to the SP-100 program. These recommendations include increasing the temperature range and preparing a realistic specimen surface.

First and foremost, the upper temperature range must be explored. While data at 1200 K is important, accurate data in the temperature region approaching 2000 K is more critical in terms of SP-100 safety engineering and core design. There are several ways to achieve the higher temperatures.

One way of increasing the temperature of the specimen would be to increase its resistance. Since the sample length is limited by the bell jar dimensions, the specimen could be split longitudinally and a smaller cross sectional area would then present a higher resistance to the current flow. Thus, the same current flow would produce more heat. Alternatively, notches could be cut near each end, serving the additional purpose of flattening the longitudinal temperature distribution (2:10).

Another solution is the use of a larger power supply. In this case, the power supply cables will become more massive and may present a dilemma when designing feed-throughs and specimen holders. A water- or nitrogen-cooled jacket could be fitted to the 00 gauge cables used in this study; care should be taken that the cooler cables do not produce a temperature gradient in the area of interest on the specimen surface from increased conduction heat loss.

A recommended approach for obtaining a more realistic specimen surface would include heating a sample of cladding in liquid lithium. If the thermocouple pigtails were attached first, the sample could be moved directly from the lithium environment into the sample holder inside the bell

jar. Providing that the lithium-treated sample would not degrade the vacuum to an unacceptable level, this would allow a comparison with previous work in order to characterize the possible effects on emittance of interactions between the coolant and the fuel cladding.

Finally, some thoughts are offered concerning oxidation and its engineering implications. One might ask why a fuel pin (and therefore an emittance measurement sample) should not be pre-oxidized in order to obtain the highest emittance possible. The reason for not using such an approach at this point is the uncertainty involved in what the core environment would do to the oxidation layer over time. Consider a possible consequence of using oxidized samples in the laboratory for obtaining the emittance value used in designing the reactor core. If the actual reactor core's environment eventually removed or otherwise adversely affected the cladding oxidation layer, the cladding emittance could decrease below the minimum level required for removing decay heat properly.

APPENDIX A: Temperature Correlations

Functions of temperature cited in this study are listed below:

Table I. Power Series Expansion for emf of Type S Thermocouples

(7:17)

<u>Temperature Range</u>	<u>Coefficients</u>	<u>Term</u>
-50 to	5.3995782346×10^0	T^1
630.74 °C	$1.2519770000 \times 10^{-2}$	T^2
	$-2.2448217997 \times 10^{-5}$	T^3
	$2.8452164949 \times 10^{-8}$	T^4
	$-2.2440584544 \times 10^{-11}$	T^5
	$8.5054166936 \times 10^{-15}$	T^6
630.74 to	$-2.9824481615 \times 10^2$	T^0
1064.43 °C	8.2375528221×10^0	T^1
	$1.6453909942 \times 10^{-3}$	T^2

Table II. Power Series Expansion for ϵ of Nb-1% Zr

(15:206)

<u>Temperature Range</u>	<u>Coefficients</u>	<u>Term</u>
400 to 2700 K	6.39×10^{-2}	T^0
	4.98×10^{-5}	T^1
	3.62×10^{-8}	T^2
	-7.28×10^{-12}	T^3

APPENDIX B: Sample Data and Calculation Results

Sample data collected for both the oxidized stainless steel (SS) emittance standard and the Nb-1% Zr specimen are shown as Tables III and IV, respectively. Table V shows an initial look at raw emittance calculation results for the SS standard prior to temperature error correction. Table VI shows the corrected results for the same specimen. Table VII shows the corrected emittance calculation results for the unoxidized Nb-1% Zr specimen.

Surface area top section:		4.7929E-04 m ² , ±5E-07 m ²									
Surface area bottom section:		4.7459E-04 m ² , ±5E-07 m ²									
Max Current		75 A									
Precision Resistor		1.33E-03 ohms, ±1% (estimated)									
% Curr	emf-1F V	emf-1R V	emf-2F V	emf-2R V	emf-3F V	emf-3R V	V-top-F mV	V-top-R mV	V-bot-F mV	V-bot-R mV	
100.101	6.1504	5.6915	5.7981	6.1049	4.9220	7.0560	285.466	285.496	285.443	285.476	
97.989	6.0338	5.5874	5.6895	5.9913	4.8356	6.9188	278.604	278.653	278.583	278.633	
96.012	5.9233	5.4876	5.5870	5.8827	4.7540	6.7886	272.182	272.253	272.155	272.230	
93.987	5.8093	5.3842	5.4815	5.7702	4.6692	6.6541	265.632	265.669	265.615	265.648	
92.040	5.6990	5.2852	5.3791	5.6626	4.5869	6.5250	259.335	259.390	259.313	259.372	
90.006	5.5824	5.1799	5.2709	5.5479	4.4995	6.3984	252.770	252.818	252.755	252.810	
87.993	5.4666	5.0756	5.1633	5.4348	4.4128	6.2531	246.296	246.346	246.283	246.330	
85.936	5.3485	4.9682	5.0535	5.3184	4.3238	6.1146	239.713	239.748	239.701	239.736	
83.907	5.2304	4.8600	4.9440	5.2015	4.2353	5.9759	233.211	233.285	233.204	233.271	
82.078	5.1237	4.7644	4.8446	5.0973	4.1541	5.5822	227.388	227.444	227.378	227.432	
79.985	5.0000	4.6519	4.7296	4.9760	4.0604	5.7082	220.724	220.793	220.717	220.782	
78.036	4.8846	4.5468	4.6219	4.8623	3.9723	5.5740	214.548	214.612	214.542	214.604	
75.961	4.7602	4.4550	4.5060	4.7394	3.8773	5.4289	207.995	208.046	207.990	208.036	
73.946	4.6385	4.3223	4.3923	4.6202	3.7838	5.2885	201.636	201.695	201.634	201.690	
71.997	4.5197	4.2139	4.2815	4.5033	3.6922	5.1509	195.523	195.569	195.521	195.560	
70.023	4.3993	4.1038	4.1689	4.3840	3.5993	5.0114	189.334	189.385	189.334	189.384	

% Curr	0 to 100% maximum current, read as 0 to 100 mV across precision resistor, $\pm 1\text{E}-06\text{ V}$
emf-1,2,3F	emf generated by thermocouple 1, 2, or 3 during "forward" polarity, $\pm 1\text{E}-04\text{ V}$
emf-1,2,3R	emf generated during "reverse" polarity, $\pm 1\text{E}-04\text{ V}$
V-top-F,R	Voltage drop between thermocouples 1 - 2, "forward" or "reverse" polarity, $\pm 1\text{E}-06\text{ V}$
V-bot-F,R	Voltage drop between thermocouples 2 - 3, $\pm 1\text{E}-06\text{ V}$

Table IV. Sample Data -- Nb-1% Zr

Surface area top section:	1.7788E-04 m ² , ±5E-07 m ²											
Surface area bottom section:	1.8941E-04 m ² , ±5E-07 m ²											
Max current:	180 A											
Precision Resistor	5.55E-04 ohms, ±1% (estimated)											
% Curr	emf-1F	emf-1R	emf-2F	emf-2R	emf-3F	emf-3R	V-top-F	V-top-R	V-bot-F	V-bot-R		
%	V	V	V	V	V	V	mV	mV	mV	mV		
39.904	5.3958	5.1609	5.2215	5.2215	5.1013	5.4809	15.2767	15.3056	16.3038	16.3433		
44.875	6.0339	5.7590	5.8269	5.9889	5.6863	6.1375	18.0362	18.0650	19.2499	19.2900		
49.770	6.5362	6.2146	6.2987	6.4759	6.1385	6.6497	20.7515	20.7703	22.1493	22.1765		
54.870	7.0170	6.6853	6.7428	6.9819	6.5615	7.1794	23.5949	23.6720	25.1800	25.2716		
59.998	7.3650	6.9365	7.0577	7.2677	6.8568	7.4880	26.3515	26.3446	28.1270	28.1240		

(Terminated at 60% maximum current due to separation of lower electrode)

Key:

% Curr 0 to 100% maximum current, read as 0 to 100 mV across precision resistor, ±1E-06 V
 emf-1,2,3F emf generated by thermocouple 1, 2, or 3 during "forward" polarity, ±1E-04 V
 emf-1,2,3R emf generated during "reverse" polarity, ±1E-04 V
 V-top-F,R Voltage drop between thermocouples 1 - 2, "forward" or "reverse" polarity, ±1E-06 V
 V-bot-F,R Voltage drop between thermocouples 2 - 3, ±1E-06 V

Table V. Sample Initial Calculation Results -- Stainless Steel (Uncorrected)

Variable Section Units	Power		Temperature		Emittance		INITIAL VALUES	
	Top [W]	Bottom [W]	Top [K]	Bottom [K]	Top N/A	Bottom N/A	Temp [K]	Emit N/A
	21.433	21.431	940.9	944.2	1.017	1.011	943	1.014
	20.477	20.476	930.3	933.5	1.017	1.012	932	1.015
	19.602	19.600	920.1	923.3	1.018	1.012	922	1.015
	18.726	18.724	909.6	912.8	1.018	1.013	911	1.016
	17.904	17.902	899.5	902.6	1.019	1.013	901	1.016
	17.065	17.064	888.6	891.9	1.020	1.014	890	1.017
	16.256	16.255	877.8	880.9	1.021	1.016	879	1.019
	15.451	15.450	866.8	869.7	1.021	1.017	868	1.019
	14.678	14.678	855.6	858.6	1.023	1.017	857	1.020
	14.000	13.999	845.6	848.5	1.023	1.018	847	1.021
	13.243	13.243	833.9	836.8	1.024	1.019	835	1.022
	12.559	12.558	822.9	825.7	1.025	1.020	824	1.023
	11.851	11.851	811.0	813.8	1.027	1.021	812	1.024
	11.184	11.184	799.3	802.1	1.028	1.022	801	1.025
	10.559	10.559	787.9	790.6	1.029	1.024	789	1.027
	9.945	9.945	776.2	778.9	1.030	1.025	778	1.028

Temperature not corrected for thermocouple--induced error

Total Surface Area of Top Section: 4.7898E-04 m²

Total Surface Area of Bottom Section: 4.7474E-04 m²

Stefan-Boltzmann Constant: 5.67051E-08

Table VI. Sample Calculation Results -- Stainless Steel (Corrected)

Variable Section Units	Power		Temperature		Emittance		REPORTED VALUES		
	Top [W]	Bottom [W]	Top [K]	Bottom [K]	Top N/A	Bottom N/A	Temp [K]	Emit N/A	± [%]
	21.433	21.431	975.7	979.0	0.878	0.874	977	0.876	3.60
	20.477	20.476	965.1	968.3	0.877	0.873	967	0.875	3.76
	19.602	19.600	954.9	958.1	0.876	0.872	957	0.874	3.92
	18.726	18.724	944.4	947.6	0.875	0.871	946	0.873	4.10
	17.904	17.902	934.3	937.4	0.874	0.870	936	0.872	4.28
	17.065	17.064	923.4	926.7	0.873	0.868	925	0.871	4.48
	16.256	16.255	912.6	915.7	0.872	0.868	914	0.870	4.70
	15.451	15.450	901.6	904.5	0.871	0.867	903	0.869	4.94
	14.678	14.678	890.4	893.4	0.870	0.866	892	0.868	5.19
	14.000	13.999	880.4	883.3	0.869	0.865	882	0.867	5.44
	13.243	13.243	868.7	871.6	0.868	0.864	870	0.866	5.74
	12.559	12.558	857.7	860.5	0.867	0.863	859	0.865	6.05
	11.851	11.851	845.8	848.6	0.865	0.861	847	0.863	6.40
	11.184	11.184	834.1	836.9	0.864	0.860	836	0.862	6.78
	10.559	10.559	822.7	825.4	0.863	0.859	824	0.861	7.17
	9.945	9.945	811.0	813.7	0.862	0.858	812	0.860	7.61

Total Surface Area of Top Section: 4.7898E-04 m²
Total Surface Area of Bottom Section: 4.7474E-04 m²
Stefan - Boltzmann Constant: 5.67051E-08

Table VII. Sample Calculation Results -- Nb -- 1% Zr

Variable Section Units	Power		Temperature		Emittance		REPORTED VALUES		
	Top [W]	Bottom [W]	Top [K]	Bottom [K]	Top N/A	Bottom N/A	Temp [K]	Emit N/A	\pm [%]
	1.098	1.172	912.5	913.1	0.159	0.159	913	0.159	1.34
	1.458	1.557	972.5	973.2	0.163	0.163	973	0.163	1.31
	1.860	1.985	1018.1	1019.0	0.173	0.173	1019	0.173	1.28
	2.334	2.491	1062.7	1063.6	0.183	0.182	1063	0.183	1.26
	2.845	3.037	1090.6	1091.6	0.200	0.200	1091	0.200	1.25

FIRST RUN (i.e. unoxidized)

Total Surface Area of Top Section: 1.7788E-04 m²

Total Surface Area of Bottom Section: 1.8941E-04 m²

Stefan - Boltzmann Constant: 5.67051E-08

Appendix C: Estimation of Errors and Uncertainties

Temperature Calculation Error

As discussed in Chapter 5, the thermocouples exhibited a known calibration error of $\delta T = -34.8$ K. Approximately one-fourth of this error, or -8 K, was due to improper preparation, i.e. using cold-worked instead of annealed thermocouple stock. Although some annealing undoubtedly occurred on the end of each thermocouple near the heated specimen, the maximum error of -34.8 K was assumed.

Tables V and VI compare the initial results with the corrected results for the Stainless Steel specimen. Table V shows the results of one experimental run without correcting for the temperature error mentioned above. Although a temperature dependence was demonstrated mathematically, the calculated emittance values were greater than unity, and thus physically meaningless. Table VI shows the same data table after correcting for δT by adding 34.8 K to each calculated value of T . All Nb-1% Zr data is shown corrected.

Uncertainties

To estimate the uncertainty in the calculated emittance values, the method outlined in ASTM C 835 was used (2:10). First, an expression was developed for calculating the uncertainty associated with each of the variables in Eq (13), using Gibbings' text "The Systematic Experiment"

(5:316). Expressed in percent, these uncertainties were calculated at each data point. The overall uncertainty in the emittance value at each point was estimated as

$$\sigma_{\epsilon_H} = (\sigma^2_{P_D} + \sigma^2_A + \sigma^2_{[T^4 - T_0^4]})^{1/2} \quad (14)$$

where each σ is the uncertainty in the respective term in Eq (13) associated with its subscript. A sample calculation is presented below for the first data point in Table VII.

First, uncertainties in the power dissipated term shall be discussed. Since a wattmeter was not used in this measurement, the power must be expressed in terms of the values measured. This is given by

$$P_D = \frac{E_R}{R_p} E_S \quad (15)$$

where

- P_D = Electric power dissipated in test region
- E_R = Voltage drop across precision resistor
- R_p = Resistance of precision resistor
- E_S = Voltage drop across test region

By applying the chain rule of differential calculus to Eq (15), one can observe how uncertainties in the independent variables will affect P_D . Here one must assume that the individual tolerances of the variables involved are equivalent to the respective standard error σ . If σ_{PD} represents the standard error in PD, then

$$\sigma^2_{P_D} = \left(\frac{\partial P_D}{\partial E_R} \sigma_{E_R} \right)^2 + \left(\frac{\partial P_D}{\partial R_P} \sigma_{R_P} \right)^2 + \left(\frac{\partial P_D}{\partial E_S} \sigma_{E_S} \right)^2 \quad (16)$$

An uncertainty for P_D may then be expressed as a percent of the value of P_D at each data point. The values used for estimating the uncertainty in P_D in the case of the first data point in Table VII are as follows:

$$\begin{aligned} P_D &= 1.135 \text{ W} \\ E_S &= 15.291 \text{ mV} \\ E_R &= 39.904 \text{ mV} \\ R_P &= 5.55\text{E-}04 \text{ ohms} \\ \sigma_{E_S} &= 1\text{E-}06 \text{ V} \\ \sigma_{E_R} &= 1\text{E-}06 \text{ V} \\ \sigma_{R_P} &= 1\% \end{aligned}$$

Next, the uncertainty in the surface area measurement shall be discussed. The formula for the surface area of the test region is $A = \pi dL$, where d is the outside diameter of the tubing and L is the length of the test region. Given that the same instrument was used to measure the lengths of the test regions and the diameter of the tubing, the uncertainty in area was estimated as twice the measurement uncertainty in one dimension. (This estimation held true for the stainless steel specimen as well, since the same instrument was used to measure the length and width of the test regions.) Since the uncertainty in one dimension was estimated as 1.0×10^{-5} inches (2.5×10^{-7} m), the estimated maximum uncertainty in surface area was $5.0 \times 10^{-7} \text{ m}^2$. Using the smaller of the two test regions for the Nb-1% Zr specimen (area of $1.7788 \times 10^{-4} \text{ m}^2$), the estimated maximum uncertainty in surface area was given by $\sigma_A / A = 0.28 \%$.

Finally, the uncertainty in the temperature term was estimated by considering both temperature averaging and voltmeter tolerance. First, the temperatures reported were in fact average test region temperatures. Although the test region was supposed to exhibit a constant surface temperature, there was a variable difference noted between adjacent thermocouples. An examination of the data revealed a maximum difference of about 4 K at any given data point. Second, the voltmeter tolerance for the range used in measuring thermocouple emf was 1×10^{-4} V, resulting in an insignificant (far less than 1 K) effect on temperature. Therefore, with a maximum 4 K spread across a test region, it was determined that a region's temperature could not be measured any more accurately than ± 2 K. This uncertainty can be expressed as a percent at each data point. However, the ASTM standard uses a format of reporting the uncertainty in the $[T^4 - T_0^4]$ term of Eq (14), which is four times the uncertainty in T.

The results of a sample calculation for estimated uncertainty is shown below in Table VIII.

Table VIII. Sample Uncertainty Estimation

Emittance	0.159
Temperature, K	913
$\sigma_{\epsilon}, \pm\%$	0.97
$\sigma_{[T^4 - T_0^4]}, \pm\%$	0.88
$\sigma_A, \pm\%$	0.28
$\sigma_{p_0}, \pm\%$	0.98
(First data point in Table VII)	

Bibliography

1. Abbott, G. L. "Total Normal and Total Hemispherical Emittance of Polished Metals," Measurement of Thermal Radiation Properties of Solids, edited by J. C. Richmond. 3-9. Washington: National Aeronautics and Space Administration, 1964.
2. American Society of Testing and Materials. "Standard Test Method for Total Hemispherical Emittance of Surfaces from 20 to 1400 °C," ASTM C 835-82 (Reapproved 1988). (December 1982).
3. Angelo, Joseph A. and David Buden. Space Nuclear Power. Malabar, FL: Orbit Book Company Incorporated, 1985.
4. Brown, Neil W. and others. "Rationale for and Design of SP-100 Auxiliary Coolant Loop," Transactions of the Sixth Symposium on Space Nuclear Power Systems. 571-575. Albuquerque: The University of New Mexico, 1989.
5. Gibbings, J. C. and others. The Systematic Experiment. Cambridge: Cambridge University Press, 1986.
6. Graves, R. S. and D. McElroy. Laboratory Notebook 316SS for Emittance Calculations, Oak Ridge, TN, August 1986.
7. Harrison, William N. "Pitfalls in Thermal Emission Studies," Measurement of Thermal Radiation Properties of Solids, edited by J.C. Richmond. 293-306. Washington: National Aeronautics and Space Administration, 1964.
8. Jet Propulsion Laboratory. Space Power News, 10: 1-4 (June 1988).
9. Jones, William and Joseph J. Kwiatowsky, Welding Development Engineers. Personal interview. EG&G Mound Technologies Facility, Dayton, OH, 21 December 1988.
10. Kao, T. "Thermal Systems Analysis Program (TSAP)," Version 1.0.1, 1982
11. Kollie, Thomas G., Staff Scientist, Telephone interview. Oak Ridge National Laboratory, Oak Ridge, TN, 15 December 1988.
12. Kollie, Thomas G. and R. S. Graves. "The Effect of Cold Working of Pt₉₀Si₁₀/Pt Thermocouples," High Temperature Thermometry Papers Presented at a Seminar at AEC Headquarters, Washington, D.C., on February 24-26, 1965.

- 13.1-13.2. Washington: Atomic Energy Commission, March 1966.
13. McElroy, D. L. and T. G. Kollie. "The Total Hemispherical Emittance of Platinum, Columbium-1% Zirconium, and Polished and Oxidized INOR-8 in the Range 100 to 1200 °C," Measurement of Thermal Radiation Properties of Solids, edited by J. C. Richmond. 365-380. Washington: National Aeronautics and Space Administration, 1964.
14. Robbins, 1Lt Donald W. An Analysis of Heat Transfer After Loss of Primary Coolant in the SP-100 Reactor System. MS thesis, AFIT/GNE/ENP/88M-8. School of Engineering, Air Force Institute of Technology (AU), Wright-Patterson AFB OH, March 1988 (AD-A194619).
15. Senor, David J. and others. "Niobium-1% Zirconium Property Correlations for Electrical Resistivity, Thermal Conductivity, Thermal Expansion, Specific Heat, and Hemispherical Total Emittance," Transactions of the Sixth Symposium on Space Nuclear Power Systems. 205-208. Albuquerque: The University of New Mexico, 1989.
16. TK Solver Plus, Academic Edition, Release 1.1. Rockford, IL: Universal Technical Systems, Incorporated, 1989.
17. U.S. Department of Commerce. Thermocouple Reference Tables Based on the IPTS-68. National Bureau of Standards Monograph 125. Washington: Government Printing Office, 1974.

Vita

John E. Thomason, III, was born on 21 October 1957 in Tupelo, Mississippi. He graduated from high school in New Albany, Mississippi, in 1975 and attended the Northeast Mississippi Community College. Majoring in physics, he transferred to the University of Mississippi in 1976 where he received the degree of Bachelor of Science in May 1979. He was employed as a research assistant at the US Department of Agriculture Sedimentation Laboratory, Oxford, Mississippi, until entering the US Air Force in January 1980. He completed pilot training in December 1980 and served as a WC-130 pilot in the 54th Weather Reconnaissance Squadron, Andersen AFB, Guam, until January 1984. He then served as a C-130 pilot, flight instructor, and wing flight safety officer in the 773rd Tactical Airlift Squadron and 463rd Tactical Airlift Wing, Dyess AFB, Texas, until entering the School of Engineering, Air Force Institute of Technology, in September 1987.

Permanent address: 13724 Greenbriar Drive
Woodbridge, Virginia 22193

REPORT DOCUMENTATION PAGE

Form Approved
OMB No. 0704-0188

Public reporting burden for this collection of information is estimated to average 1 hour per response, including the time for reviewing instructions, searching existing data sources, gathering and maintaining the data needed, and completing and reviewing the collection of information. Send comments regarding this burden estimate or any other aspect of this collection of information, including suggestions for reducing this burden, to Washington Headquarters Services, Directorate for Information Operations and Reports, 1215 Jefferson Davis Highway, Suite 1204, Arlington, VA 22202-4302, and to the Office of Management and Budget, Paperwork Reduction Project (0704-0188), Washington, DC 20503.

1. AGENCY USE ONLY (Leave blank)		2. REPORT DATE December 1992	3. REPORT TYPE AND DATES COVERED Master's Thesis	
4. TITLE AND SUBTITLE TOTAL HEMISPHERICAL EMITTANCE OF NIOBIUM - 1% ZIRCONIUM FUEL CLADDING FOR THE SP-100 SPACE REACTOR			5. FUNDING NUMBERS	
6. AUTHOR(S) JOHN E. THOMASON, III				
7. PERFORMING ORGANIZATION NAME(S) AND ADDRESS(ES) AIR FORCE INSTITUTE OF TECHNOLOGY WRIGHT-PATTERSON AFB, OH 45433			8. PERFORMING ORGANIZATION REPORT NUMBER AFIT/GNE/ENP/92D-1	
9. SPONSORING/MONITORING AGENCY NAME(S) AND ADDRESS(ES)			10. SPONSORING/MONITORING AGENCY REPORT NUMBER	
11. SUPPLEMENTARY NOTES				
12a. DISTRIBUTION/AVAILABILITY STATEMENT Approved for public release; distribution unlimited.			12b. DISTRIBUTION CODE	
13. ABSTRACT (Maximum 200 words) Total hemispherical emittance was measured for the SP-100 reactor fuel cladding alloy (Nb-1% Zr). Based on a standard test method (ASTM C 835-82), experiments were conducted on a reference sample of oxidized stainless steel and then on a sample of actual cladding. The sample is heated in a vacuum by passing DC current through it until reaching equilibrium. Measurements are made of the electrical power dissipated in the sample and of the surface temperature. Using the Stefan-Boltzmann Law and some key assumptions concerning conductive and radiative heat transfer, the measured quantities are used to calculate emittance. Calculated values for unoxidized cladding range from $0.159 \pm 5.35\%$ at 913 K to $0.200 \pm 4.51\%$ at 1091 K. Highest value measured after onset of visible oxidation was $0.339 \pm 3.92\%$ at 1269 K.				
14. SUBJECT TERMS SP-100, reactor, emittance, niobium, fuel cladding, emissivity			15. NUMBER OF PAGES 67	
			16. PRICE CODE	
17. SECURITY CLASSIFICATION OF REPORT Unclassified	18. SECURITY CLASSIFICATION OF THIS PAGE Unclassified	19. SECURITY CLASSIFICATION OF ABSTRACT Unclassified	20. LIMITATION OF ABSTRACT UL	